Electronic Supplemental Information

Molecularly-Tunable Nanoelectrode Arrays Created by Harnessing Intermolecular Interactions

Han-Wen Cheng[a,b]*, Shan Wang[b], Marc D. Porter[c]*, and Chuan-Jian Zhong[b]*

[a)] School of Chemical and Environmental Engineering, Shanghai Institute of Technology, Shanghai 201418, China
[b)] Department of Chemistry, State University of New York at Binghamton, Binghamton, New York 13902, USA
[c)] Department of Chemistry and Chemical Engineering, University of Utah, Salt Lake City, Utah 84112, USA

Additional experimental data and data analysis:

Table S1 Summary of the binding strength estimated based on density functional theory (DFT)-calculated E_b*[1,2] for the selected thiolate molecules ($CH_3(CH_2)_{n-1}SH$) on gold surfaces.

Thiolate molecules	E_b* (eV)	
FTP	-3.43	Linear extrapolation based on "electronegativity *vs*. E*" (E_b = -0.6449×*n* -0.8533)
MHA	-4.39	Linear regression based on Ref. [1] (E_b = -0.1043× *n* -2.6286)
MBA	-2.56	Ref. [2]
TP	-2.20	Ref. [2]
ET	-2.61	Ref. [2]
MUA	-3.48	Linear regression based on Ref. [1] (E_b = -0.1043× *n* -2.6286)
HDT	-4.0392	Linear regression based on Ref. [1] (E_b = -0.1063× *n* -2.3384) [2]

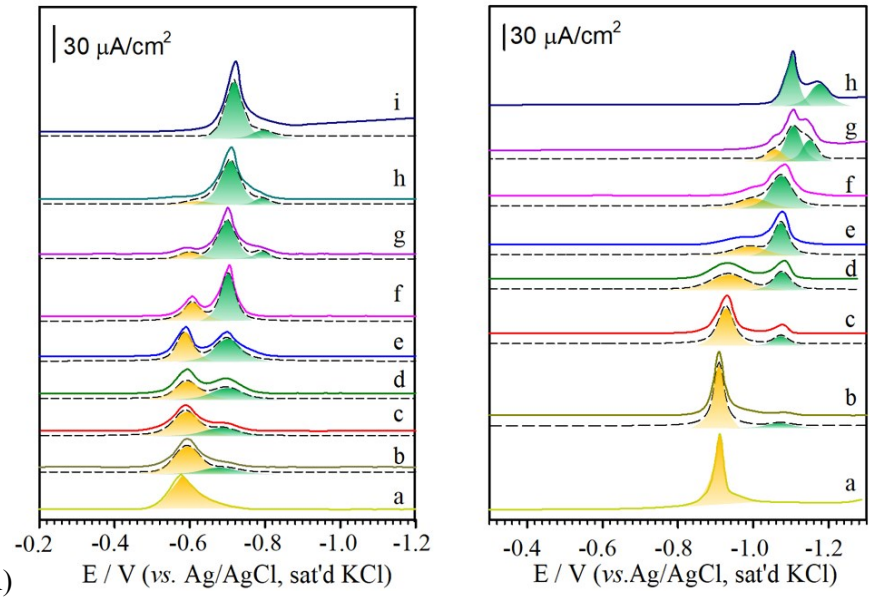

Fig. S1 Voltammetric curves (dashed and colored curves represent deconvoluted waves). (A) TP/ET: (a) TP (E_p= -0.58 V). (b), (c), (d), (e), (f), (g), and (h) TP/ET (mixing ratios: 30, 15, 10, 5, 2, 0.5, and 0.1 with a total thiol concentration of 5.0 mM. E_p: -0.59 and -0.69 V (b); -0.59 and -0.69 V (c); -0.59 and -0.70 V (d); -0.60 and -0.70 V (e); -0.61 and -0.70 V (f); -0.61, -0.70 and -0.78 V (g) and -0.61, -0.71 and -0.78 V (h)). (i) ET (E_p= -0.72 and -0.78 V). The more negative potential wave corresponds to the monolayer of ET (-0.72 V) which has a narrower width (45 mV) than those for the TP-derived monolayer (-0.58 V, 85 mV) reflects a difference in adsorbate-adsorbate interaction. (B) MUA/HDT: (a) MUA (E_p = -0.89 V). (b), (c), (d), (e), (f), and (g) MUA/HDT (mixing ratios: 18.0, 9.0, 6.0, 3.5, 2.0, and 1.0 with a total thiol concentration of 2.5 mM. E_p: -0.91V and -1.08 V (b), -0.94 and -1.08 V (c), -0.94 and -1.09 V (d), -0.96 and -1.08 V (e), -0.99, and -1.08 (f), -1.05 V, -1.10 and -1.14 V (g)). (h) HDT (E_p: -1.11 and -1.17 V). (Electrolyte: 0.5 M KOH, Geometric surface area of electrode: 0.6

cm^2, scan rate: 50 mV/sec). In comparison with the single wave characteristic at the less negative potential (E_p = -0.89 V) for MUA monolayer, HDT monolayer features a double-wave character at the more negative potential (h), -1.11 V and -1.17 V, which is consistent with earlier finding[3] on the voltammetric desorption potentials as a function of the number of carbons (n) in the alkyl chain.

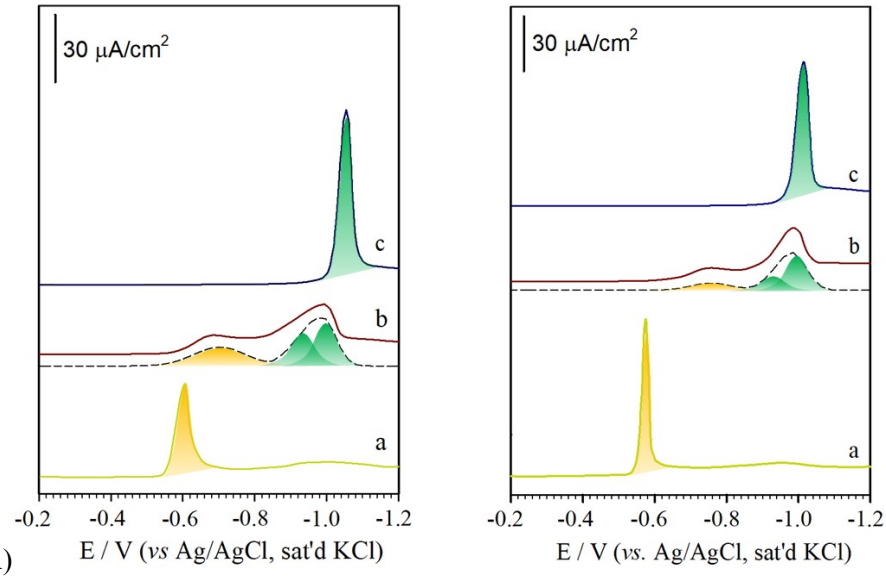

Fig. S2 Voltammetric curves: (A) (a) FTP (E_p (FTP) = -0.60 V), (b) FTP/MHA (FTP/MHA mixing ratio: 25 with a total thiol concentration of 3.5 mM (E_p (FTP)= -0.68 V and E_p (MHA)= -1.0 V)), and (c) MHA (E_p (MHA)= -1.06 V). (B) (a) MBA (E_p (MBA)= -0.57 V), (b) MBA/MHA (MBA/MHA mixing ratio: 20 and a total thiol concentration of 3.4 mM (E_p (MBA)= -0.78 V and E_p (MHA)= -0.99 V)), and (c) MHA (E_p (MHA)= -1.06 V). (Electrolyte: 0.5 M KOH, Geometric surface area of the electrode: 0.6 cm^2, and Scan rate: 50 mV/sec).

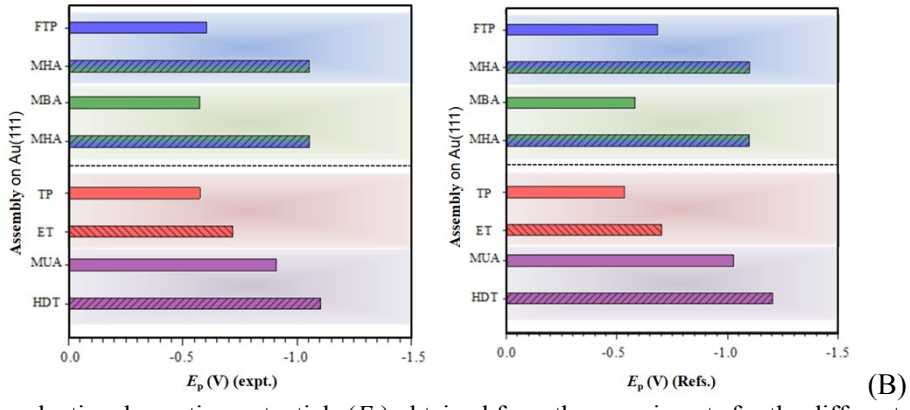

Fig. S3 (A) Plot of the reductive desorption potentials (E_p) obtained from the experiments for the different pairs of molecules studied in this work. ($E_{p(Ag/AgCl)}$). (B) Reductive desorption potentials (E_p) estimated based on literature reports for different thiolate molecules on gold surfaces: FTP's $E_{p(SCE)}$ = -0.73 V (based on fitting[2]); MHA's $E_{p(SCE)}$ = -1.15 V (based on fitting[2]); MBA's $E_{p(SCE)}$ = -0.63 V[4]; TP's $E_{p(SCE)}$ = -0.58V[5]; ET's $E_{p(SCE)}$ = -0.75 V[6]; MUA's $E_{p(SCE)}$ = -1.08 V (based on fitting[2]); and HDT's $E_{p(SCE)}$ = -1.25 eV (based on fitting[2]). Note that the potential is give in $E_{p(Ag/AgCl)}$, which is - 0.05 V with respect to $E_{p(SCE)}$.

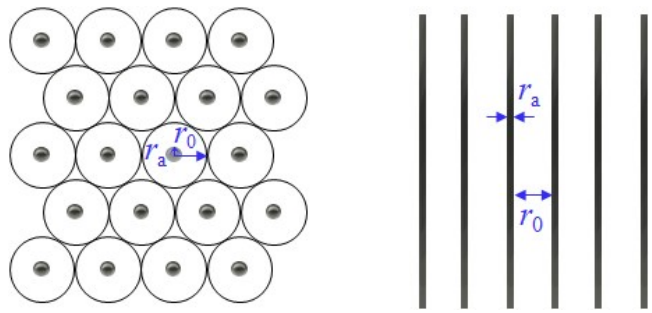

(A) (B)

Scheme S1. Simulation models of the nanoelectrode arrays: disk-shaped (A) and strip-shaped (B) models. Simulation of nanoelectrode array is based on the dimensionless equation of current (*i*) ~ potential (*E*) derived by Amatore *et al.*[7]**:**

For disk-type:

$$r_a = r_0(1-\theta)^{1/2} \tag{1}$$

For stripe-type:

$$r_a = r_0(1-\theta) \tag{2}$$

Dimensionaless equation of current ~ potential:

$$\Psi = \Lambda(1-\theta)\exp(\alpha\xi)\left\{\left[1 - I\Psi - 2r\Psi f(1-\theta)\right] - \left[I\Psi + 2r\Psi f(1-\theta)\right]\exp(-\xi)\right\} \tag{3}$$

where

$$r = r_a\left(\frac{DRT}{F\upsilon}\right)^{-1/2} \tag{4}$$

$$\Lambda = k_0\left(\frac{RT}{DF\upsilon}\right)^{1/2} \tag{5}$$

$$\xi = -\frac{F}{RT}(E - E^0) \tag{6}$$

$$\tau = \frac{F}{RT}\upsilon t \tag{7}$$

$$\Psi = \frac{i}{FAC^0\left(\frac{DF\upsilon}{RT}\right)^{1/2}} \tag{8}$$

$$I\Psi = \frac{1}{\sqrt{\pi}}\int_0^{\tau}\frac{\Psi}{(\tau-\eta)^{1/2}}d\eta \tag{9}$$

The $f(1\text{-}\theta)$ function is

$$f(1-\theta) = 0.3(1-\theta)^{-1/2} \quad \text{for disk-type} \tag{10}$$

and

$$f(1-\theta) = 1 - \frac{1}{\sqrt{\pi}}\ln\left[\frac{\pi}{2}\sin(1-\theta)\right] \quad \text{for stripe-type} \tag{11}$$

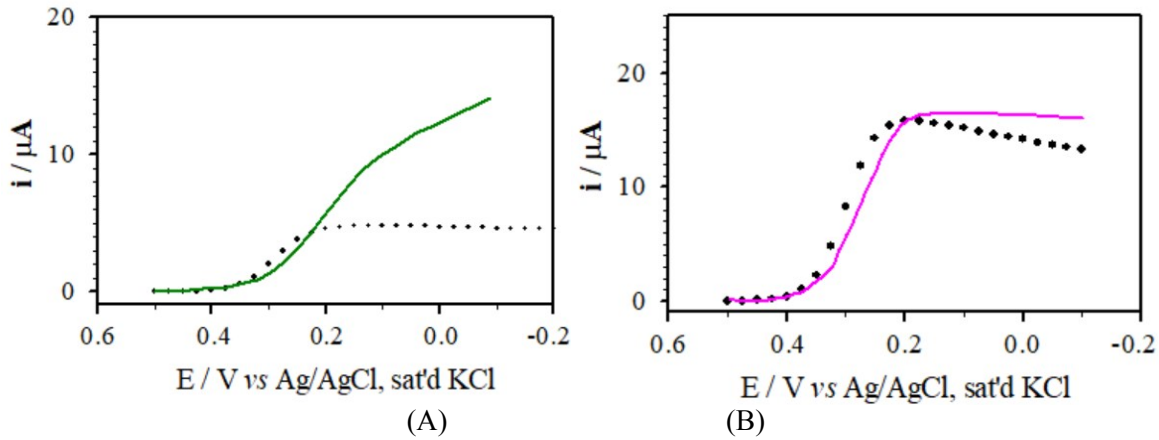

Fig. S4 Theoretical modeling results for the reduction of $Fe(CN)_6^{3-}$ on the perforated MUA/HDT (A) and MBA/MHA (B). (A) The comparison of experimental data (lines) from Fig. 4A (c) with the simulation (points) in strip-model using r_a= 1.23 nm, R_0= 2.05×10^4 nm ($1-\theta$=6.0×10^{-5}), D= 1.12×10^{-6} cm^2/s, and k =2. (B) The comparison of experimental data (lines) from Fig. 4A (d) with the simulation (points) in strip-model using r_a= 2.74 nm, R_0= 6.09×10^3 nm ($1-\theta$=5.0×10^{-4}), D= 1.12×10^{-6} cm^2/s, and k =2.

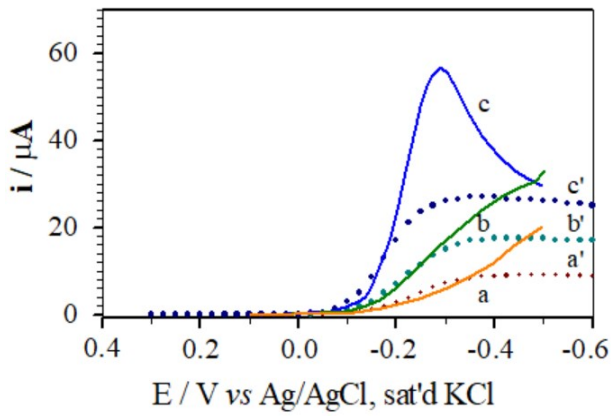

Fig. S5 Theoretical modeling results for reduction of $Ru(NH_3)_6^{3+}$ at three different pH values on the perforated MBA/MHA system. The comparison of experimental data (lines: a, b, and c) from (Fig. 4B (b-d)) with the simulation (points: a', b', and c') in strip-model using r_a= 0.5 nm, R_0= 5.57×10^4 nm ($1-\theta$=8.0×10^{-1}), D= 7.5×10^{-6} cm^2/s, and k= 2 for pH~3.4 (a); r_a= 0.9 nm, R_0= 3.75×10^4 nm ($1-\theta$=2.5×10^{-5}), D= 1.1×10^{-5} cm^2/s, and k= 2 for pH~6.0 (b); and r_a= 0.4 nm, R_0= 3.75×10^4 nm ($1-\theta$ =1.03×10^{-4}), D= 1.7×10^{-5} cm^2/s, and k= 2 for pH~10.3 (c).

Table S2. Summary of parameters for nanoelectrode array simulation (disk-model Fig. 4D-E).

	Perforated Film	r_a (nm)	R_0 (nm)	$1-\theta$	i_{theory} (μA)	$i_{simulated}$ (μA)	N_μ
(i) $Fe(CN)_6^{3-}$	MUA/HDT	2	482	8.62×10^{-6}	3.21×10^{-7}	3.08×10^{-7}	4.39×10^7
(ii) $Fe(CN)_6^{3-}$	MBA/MHA	20	1950	1.05×10^{-4}	3.21×10^{-6}	3.07×10^{-6}	5.35×10^6
(iii) $Ru(NH_3)_6^{3+}$	MBA/MHA	7.5	2160	1.21×10^{-5}	7.53×10^{-6}	5.71×10^{-6}	4.38×10^6

Note: Data for i, ii and iii are the data from Fig. 4D (a), 4D (b) and 4E (b). $i_{theory} = 4nFDC^0 r_a$; $i_{simulated} = I_{lim} / \#N$ where $N_\mu = A_{total}/A_{singl} = A_T/\pi R_0^2 = A_T(1-\theta)/\pi r_a^2$, A_T = 0.64 cm^2. (see Fig. S6 for single nanoelectrode limiting current.)

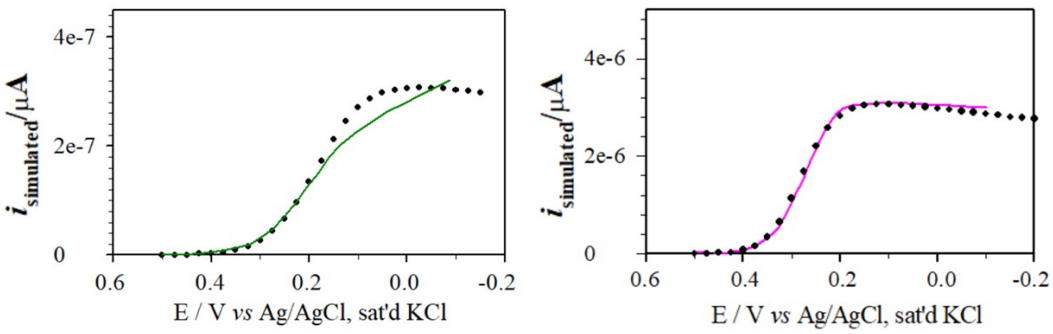

(A) (B)

Fig. S6 Comparison between the experimental (line) and simulated (point, disk-model) steady state limiting current based on eqn. 5. (A) Perforated MUA/HDT, (B) perforated MBA/MHA monolayer (Electrolyte: 1 M KCL with 1.3 mM $Fe(CN)_6^{3-}$).

References:

1. D. Nassoko, M. Seydou, C. Goldmann, C. Chanéac, C. Sanchez, D. Portehault, F. Tielens. Rationalizing the formation of binary mixed thiol self-assembled monolayers, *Mater. Tod. Chem.*, 2017, **5**, 34-42.
2. R. C. Salvarezza, P. Carro. The electrochemical stability of thiols on gold surfaces. *J. Electroanal. Chem.*, 2018, **819**, 234–239.
3. C. J. Zhong, M. D. Porter, The fine structures of voltammetric curves for the electrochemical desorption of organosulfur-based monolayers at gold, *J. Electroanal. Chem.*, 1997, **425**, 147.
4. M. C. R. González, A. G. l. Orive, P. Carro, R. C. Salvarezza, C. Ahn, Structure and electronic and charge-transfer properties of mercaptobenzoic acid and mercaptobenzoic acid–undecanethiol mixed monolayers on Au (111), *J. Phys. Chem.* 2014, **118**, 30013–30022.
5. H. Kang, J. Noh, Influence of thiol molecular backbone structure on the formation and reductive desorption of self-assembled aromatic and alicyclic thiol monolayers on Au(111) surface, *Bull. Kor. Chem. Soc.* 2013**, 34**, 1383–1387.
6. S. Imabayashi, M. Iida, D. Hobara, Z. Q. Feng, K. Niki, T. Kakiuchi, Reductive desorption of carboxylic-acid-terminated alkanethiol monolayers from Au(111) surfaces, *J. Electroanal. Chem*. 1997, **428**, 33–38.
7. C. Amatore, J. M. Saveant, D. Tessier, Charge transfer at partially blocked surfaces: A model for the case of microscopic active and inactive sites, *J. Electroanal. Chem*., 1983, **147**, 39-51.